World Journal of Advanced Research and Reviews
eISSN: 2581-9615 CODEN (USA): WJARAI
Cross Ref DOI: 10.30574/wjarr
Journal homepage: https://wjarr.com/

(RESEARCH ARTICLE)

Check for updates

# Molecular dynamics exploration of protein–ligand interactions between c-kit and three benzothiazole-2-thiol derivatives

Neantien Thilerien YAO BI [1, *], Latifatou laye ALAO [1], Charles Kouman Koffi [2], Sékou DIOMANDE [3] and Soleymane KONE [1]

[1] *Department of Sciences of Structure and Matter (SSMT), Laboratory of Constitution and Reaction of Matter (LCRM), University of Félix Houphouët-Boigny, Abidjan, Ivory Coast.*
[2] *Laboratory of Fundamental and Applied Physics, University of Abobo-Adjamé (now Nangui ABROGOUA), Abidjan Autoroute d'Abobo, Abidjan 02, Côte d'Ivoire.*
[3] *Department of Agro-Industrial Sciences and Technologies (AIST), UFR Agriculture, Halieutic Resources and Agro-Industry (AHRAI), University of San Pedro, San Pedro, Ivory Coast.*

World Journal of Advanced Research and Reviews, 2026, 29(03), 1865-1880

Publication history: Received on 17 February 2026; revised on 23 March 2026; accepted on 26 March 2026

Article DOI: https://doi.org/10.30574/wjarr.2026.29.3.0739

## Abstract

The c-kit tyrosine kinase receptor is a strategic therapeutic target involved in regulating signaling pathways that control tumor proliferation and survival. This study used a computational approach to explore protein-ligand interactions between c-kit and three benzothiazole-2-thiol derivatives (LIG24, LIG26, and LIG32) in order to identify drug candidates.

SwissADME software was used to estimate the pharmacokinetic properties (ADME) for this study. The electronic properties were evaluated using DFT calculations at the B3LYP/6-311++G(d,p) theory level with Gaussian 09 software. For the stability of c-kit-ligand complexes and ligand interactions in the c-kit catalytic pocket, a molecular dynamics simulation was performed using Desmond software over a period of 200 ns.

For each ligand, the results reveal pharmacokinetic profiles compatible with therapeutic application. All three complexes exhibit stability with stationary RMSD plateaus. The C-KIT–LIG26 complex stands out with the lowest potential energy. This complex exhibits a network of persistent interactions involving key residues in the active site (LYS623, ILE789, ASP810, and VAL654).

Finally, the results obtained indicate that the LIG26 ligand is a good drug candidate for developing a c-kit-targeting inhibitor for the treatment of HCC.

**Keywords:** c-Kit; Protein Residue; Ligand; Molecular Dynamics; ADME; Interactions

## 1. Introduction

Hepatocellular carcinoma (HCC) is one of the leading causes of cancer-related mortality worldwide. It remains characterized by a limited therapeutic response to conventional treatments. In this context, identifying new molecular targets and developing more selective inhibitors are major priorities in oncology. Among these targets, the c-kit protein, a receptor tyrosine kinase, has a key role in regulating fundamental biological processes. Activation of c-kit triggers several intracellular signaling cascades, including the Ras/ERK, PI3K/Akt, and JAK/STAT pathways, which control cell proliferation, survival, differentiation, and tumor angiogenesis [1]. However, when this regulation is impaired, aberrant

* Corresponding author: YAO BI Neantien Thilerien

c-kit signaling promotes tumor growth and malignant progression, making this receptor a strategic therapeutic target (D) [2].

After demonstrating significant anticancer activity on the HepG2 hepatocellular cell line [3], benzothiazole-2-thiol derivatives have recently emerged as promising candidates. Although these in vitro results are encouraging, the precise molecular mechanisms of their interaction with the catalytic domain of c-kit remain largely unexplained. However, preclinical validation of a drug candidate requires not only high binding affinity, but also sustained interactional stability over time. The pharmacokinetic profile of the drug candidate must also be compatible with effective systemic administration.

This study is based on multiscale molecular modeling, combining biomedical analyses and appropriate computational methods. Three benzothiazole-2-thiol derivatives were evaluated.

Our goal is to use an integrated computational strategy to evaluate the inhibitory potential and pharmacokinetic safety profile of the three benzothiazole-2-thiol derivatives. Specifically, this study aims to (i) predict their absorption, distribution, metabolism, and excretion (ADME) and electronic properties, (ii) analyze the structural and dynamic stability of protein-ligand complexes, and (iii) finely characterize the dominant non-covalent interactions.

Various software programs were used to achieve these specific objectives. First, SwissADME software was used to predict the ADME properties and potential oral bioavailability of these derivative kings (ligands). Next, Gaussian 09 was used to analyze the electronic properties. Finally, a molecular dynamics simulation was performed using Desmond software. This dynamic approach made it possible to realistically reproduce the conformational fluctuations of the protein-ligand complex under conditions close to those found in the physiological environment.

## 2. Target protein, ligands, and calculation methods.

### 2.1. Target protein (C-KIT receptor)

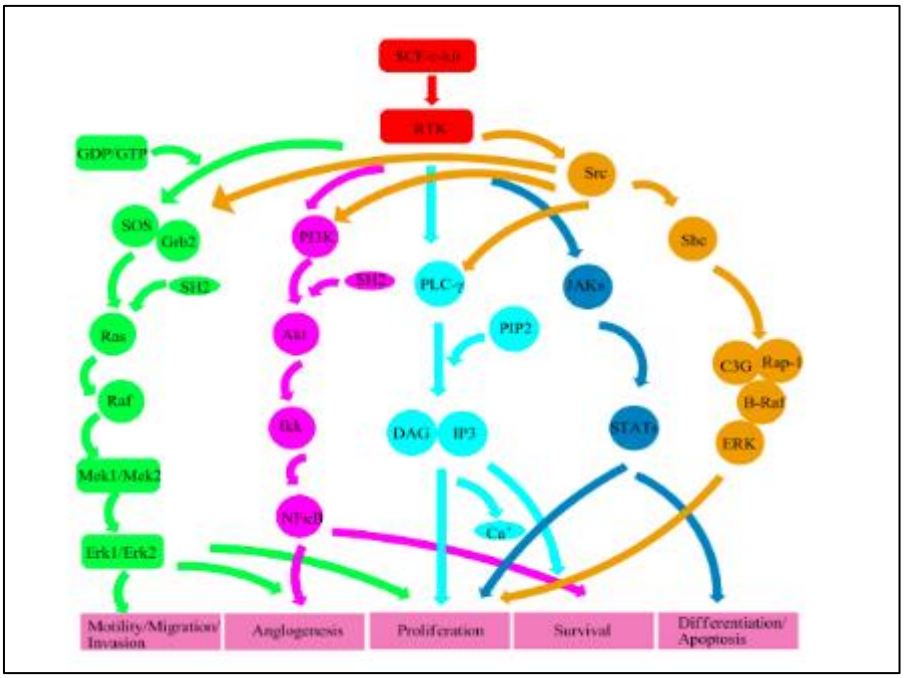


• Ras/Erk pathway (MAPK): activated via the Grb2 and Sos proteins, it controls proliferation, angiogenesis, migration, and motility.; • PI3K/Akt pathway: recruited by PI3K SH2 domains, it promotes cell survival and angiogenesis.; • PLC-γ pathway: generates second messengers (DAG, IP3) leading to PKC activation and increased intracellular calcium, which are essential for proliferation and survival.; • Src kinase pathway: modulates migration, motility, invasion, and angiogenesis, playing a key role in tumor progression.; • JAK/STAT pathway: activates transcription factors involved in proliferation, differentiation, and apoptosis regulation.

**Figure 1** Diagram showing the main signaling pathways activated by the c-kit receptor: Ras/Erk, PI3K/Akt, PLC-γ, Src kinase, and JAK/STAT, and their effects on cell proliferation, survival, and differentiation

C-kit (CD117) receptor is a transmembrane protein belonging to the tyrosine kinase receptor family. Its natural ligand, stem cell factor (SCF), induces its dimerization and autophosphorylation. This leads to the activation of multiple intracellular proteins. These partner proteins act as relays, triggering diverse and complementary signaling pathways. Figure 1 shows the main signaling pathways activated by the c-kit receptor. These pathways include Ras/Erk, PI3K/Akt, PLC-γ, Src kinase, and JAK/STAT, as well as their effects on cell proliferation, survival, and differentiation.

Thus, c-kit acts as a signaling platform, where several molecular cascades converge and coordinate. These interactions explain its crucial role in:

*2.1.1. Usefulness of the c-kit receptor and its role in cancer treatment*

C-KIT (CD117) receptor plays a central role in fundamental biological processes. Under physiological conditions, its activation by stem cell factor (SCF) maintains the balance of hematopoietic stem cells, melanocytes, mast cells, and germ cells.

However, in a pathological context, activating mutations of c-kit induce constitutive signaling independent of the presence of its ligand [4]. This permanent activation promotes uncontrolled proliferation and apoptotic evasion, key mechanisms of malignant transformation. Such alterations are found in several cancers, including gastrointestinal stromal tumors (GIST), certain myeloid leukemias, systemic mastocytosis, and certain melanomas [5].

Therefore, this oncogenic dependence on c-kit has made this receptor a prime therapeutic target. Tyrosine kinase inhibitors (TKIs), such as imatinib, sunitinib, and regorafenib, have demonstrated significant clinical efficacy by inhibiting the enzymatic activity of c-kit, leading to reduced tumor growth and improved patient prognosis [6]. These targeted therapies have transformed the management of patients with GIST and other c-kit-related cancers, significantly improving their survival.

Thus, the c-kit receptor is not only a major player in cell biology, but also a strategic anchoring point in oncology. In-depth knowledge of this receptor not only explains the origin of certain tumors, but also paves the way for personalized treatments based on selective inhibition of its signaling.

### 2.2. Benzothiazole-2-thiol derivatives (ligands)

The 2D and 3D structures of the three benzothiazole-2-thiol derivatives selected as ligands are summarized in Table 1 below:

**Table 1** 2D structures, optimized 3D structures, and designations of the three selected ligands

| 2D Structure | 3D Structure | Designation |
|---|---|---|
| 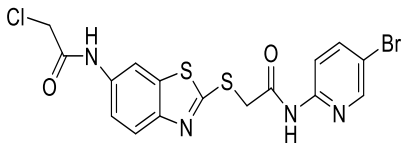 | 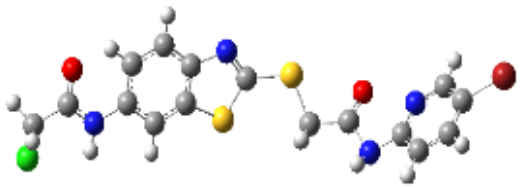 | LIG24 |
| 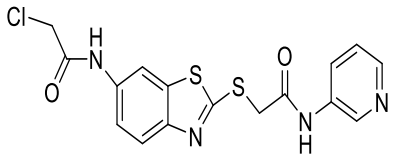 | 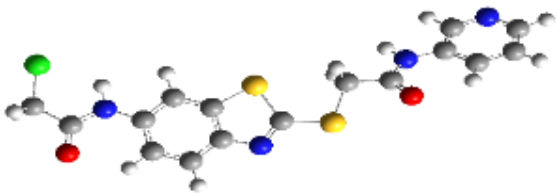 | LIG26 |
| 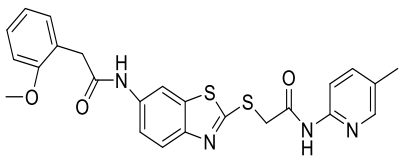 | 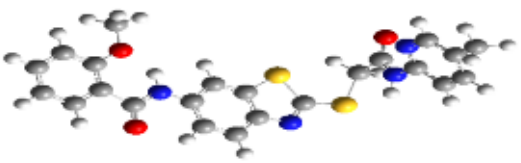 | LIG32 |

Below is a description of the methodology used to conduct this study, from the evaluation of ADME properties to molecular dynamics simulations of ligands in a biological environment.

## 3. Methodology

There are two main steps in the methodology. The first step is all about calculating the molecular parameters of the ligands. In the second step, we calculate the parameters of the protein-ligand interactions.

The first step begins with the construction of the molecular structure of each ligand in the dedicated interface of the SwissADME software. This structure is automatically converted into SMILES notation. This is followed by systematic evaluation calculations of ADME parameters. These calculations lead to several key molecular descriptors. These include molar mass, lipophilicity (LogP), the number of hydrogen bond donors and acceptors (HBD and HBA), topological polar surface area (TPSA), and compliance with Lipinski's rules (HBD ≤ 5, HBA ≤ 10, molar mass < 500 Da, and LogP < 5) [7].

Concomitant with the pharmacokinetic analysis, the optimal structures of the three ligands were calculated using Gaussian software. The density functional theory (DFT) approach was chosen to perform these calculations. This method is recognized for handling a large part of the electronic correlation. The theoretical level chosen was B3LYP/6-311++G(d,p) [8]. These calculations were performed in two phases : gaseous and aqueous. They provided access to the dipole moment values of each ligand in these phases.

The second step evaluates the dynamic stability of the ligand–C-KIT complexes. To this end, the three complexes from the docking studies were imported into the Desmond software, integrated into the Schrödinger suite. Each complex was then immersed in a cubic box of explicit TIP3P water, respecting a margin of 10 Å around it. In addition, the systems were neutralized by adding $Na^+$ and $Cl^-$ ions to reproduce a physiological ionic concentration of 0.15 M [9].

Simulations were conducted in the isothermal-isobaric (NPT) ensemble, at a temperature of 300 K and a pressure of 1 bar. The equations of motion were integrated using the Verlet algorithm, with a time step of 1.5 fs, while temperature and pressure control were applied in accordance with standard protocols. Interatomic interactions were described using the OPLS4 force field, with a truncation distance of 14 Å for non-bonding interactions. Finally, each complex underwent a 200 ns production simulation.

## 4. Results and Discussion

### 4.1. Physicochemical and pharmacokinetic properties

Certain physicochemical and pharmacokinetic properties of ligands LIG24, LIG26, and LIG32 were evaluated according to the procedure described in section 2.3. These include the dipole moment (μ) values in the gas and aqueous phases, lipophilicity or LogP coefficient, number of hydrogen bond donors (HBD) and acceptors (HBA), molecular mass, topological polar surface area (TPSA) and molar refraction (R_m). These data are compiled in Table 2.

**Table 2** Dipole moment values (μ in Debye) and ADME pharmacokinetic parameters (LogP, HBA, HBD, TPSA in $Å^2$, molecular weight in g/mol, and $\boldsymbol{R_m}$) calculated for the three ligands studied.

| **Properties** | **LIG24** | **LIG26** | **LIG32** |
|---|---|---|---|
| $\mu_{aq}$ | 7.61 | 12.77 | 14.11 |
| $\mu_g$ | 7.31 | 4.30 | 4.16 |
| $LogP$ | 3.44 | 2.55 | 4.31 |
| HBA | 4 | 4 | 5 |
| HBD | 2 | 2 | 2 |
| molecular weight | 471.78 | 392.88 | 478.59 |
| TPSA ($Å^2$) | 137.52 | 162.82 | 155.98 |
| $R_m$ | 109.78 | 112.46 | 136.28 |

Physico-chemical and pharmacokinetic parameters of the three benzothiazole-2-thiol-derived ligands (LIG24, LIG26, and LIG32) reveal different characteristics.

The dipole moments of the two ligands LIG26 and LIG32 are very high in aqueous media. Compared to those in the gas phase, these parameters have practically tripled. It follows that in the presence of water molecules, interactions between these ligands and the polar residues of the active site could be favored. The low values in the gas phase reflect the influence of the solvent (water) on this molecular property of these ligands. In contrast, the LIG24 ligand exhibits moderate polarity and is virtually stable in both phases. The dipole moment of this ligand is 7.61 D in aqueous media and 7.31 D in gaseous media. This is an advantage in terms of conformational robustness and stability in different environments.

Lipophilicity values reflect contrasting profiles. According to Lipinski's criteria, for a ligand to be bioavailable, its lipophilicity must be less than 5 (LogP<5). All three ligands satisfy this condition. The LIG32 ligand, with the highest LogP value (4.31), is particularly suited to hydrophobic interactions. This behavior comes at the expense of its aqueous solubility, which could reduce its bioavailability. However, the LIG26 ligand, which is more hydrophilic (lower LogP value : 2.55), has better solubility and circulates more easily in biological media. The LIG24 ligand has an intermediate profile, reflecting a good balance between solubility and lipophilicity. This supports generally favorable pharmacokinetic behavior [10].

Furthermore, the three ligands have two hydrogen bond donors (HBD). However, the LIG32 ligand has one additional acceptor compared to the LIG24 and LIG26 ligands (5 HBA compared to 4). This could be an advantage that improves its specific recognition at the active site.

The differences between molecular weight and topological polar surface area (TPSA) values allow for further refinement of the interpretation. The LIG26 ligand is the lightest (392.88 g/mol) and has the largest topological polar surface area. Consequently, it has increased mobility and flexibility, which are favorable for conformational adaptation [11]. Nevertheless, its high TPSA (162.82 $Å^2$) exceeds the optimal threshold of 140 $Å^2$, thereby limiting its membrane permeability and thus its potential for cellular diffusion [12]. A similar trend is observed for LIG32 (TPSA = 155.98 $Å^2$). In contrast, LIG24, with a TPSA of 137.52 $Å^2$, remains below the critical threshold, which promotes its ability to cross biological membranes and improves its bioavailability.

Molar refraction is an indication of a molecule's polarizability. The calculated values confirm the differences between the three ligands. Ligand LIG32 has the highest value (136.28). It is more susceptible to Van der Waals interactions, particularly within hydrophobic regions. In comparison, LIG26 (112.46) and LIG24 (109.78) have more moderate values, consistent with their more equilibrated profiles.

### 4.2. Energy properties and stability of complexes

This section presents the results of the second stage of the calculation methodology. Molecular dynamics simulations of the interactions between each ligand and the c-kit receptor were performed at a temperature of 300 K. These calculations, lasting 200 nanoseconds for each system, made it possible to explore the conformational space of the ligand. They yielded average values for the total energy ($E_m$) and potential energy ($E_p$)of each complex. Table 3 shows the results of these energy values for the complexes :

**Table 3** Energy and Thermal Parameters (in kcal/mol) of the Three C-KIT-Ligand Complexes

| Property of the Complex | C-KIT-LIG24 | C-KIT-LIG26 | C-KIT-LIG32 |
|---|---|---|---|
| Atoms of the complex | 40 379 | 40394 | 40381 |
| $E_m$ | -101953.64 | -101992.36 | -101888.32 |
| $E_p$ | -126715.70 | -126765.89 | -126653.25 |

These results show really negative average total energies. This means strong thermodynamic stability **[13]**. Complex with ligand LIG26 has the lowest total energy (-101992.36 kcal/mol) and complex with LIG32 has the highest (-101888.32 kcal/mol). These results suggest that LIG26 binds with greater affinity to the protein.

The average potential energies confirm this trend. These energy values are lower than the total energies. In the complexes formed between the receptor and ligands LIG26, LIG24, and LIG32, the average potential energies are -

126765.89 kcal/mol, -126715.70 kcal/mol, and -126653.25 kcal/mol, respectively. These values are consistent with the principles established by Levitt and Warshel (1975), according to which such energies reflect the stability of a molecular system. The temperature is set at 300 K in accordance with physiological conditions **[14]**.

Taken together, the three ligands form stable complexes with c-kit. The complex obtained with the LIG26 ligand is the most stable. Structural evolution by RMSD, identification of specific bonds, and local flexibility by RMSF were performed to investigate differences in stability and interactions between the complexes.

### 4.3. RMSD analysis of the three C-KIT-Ligand complexes

The Root Mean Square Deviation (RMSD) is a widely used approach in molecular dynamics to evaluate conformational stability, trajectory convergence, and the robustness of protein-ligand complexes over time **[15]**. Figures 2, 3, and 4 show the evolution of the RMSD for the three complexes studied.

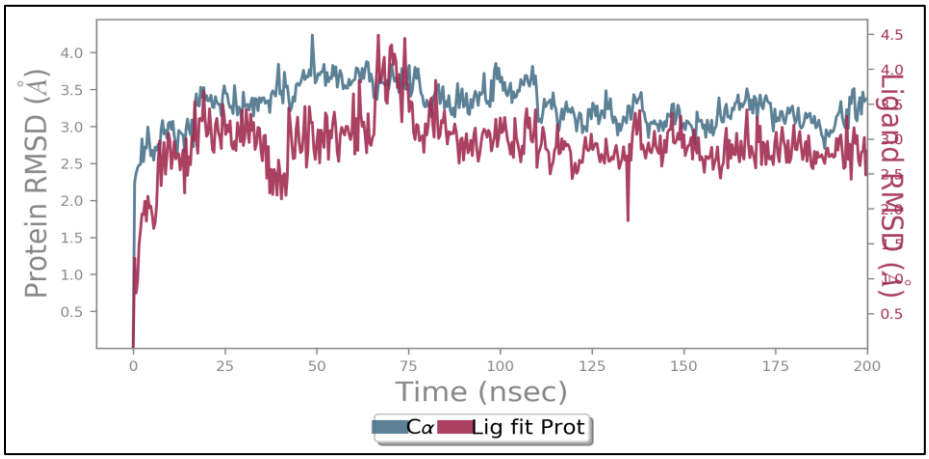


**Figure 2** Evolution of the RMSD of the C-KIT-LIG26 complex

In this complex, the RMSD of the protein increases rapidly at the start of the simulation. This explains an initial structural relaxation of the receptor in response to the presence of the ligand. This fact reflects a gradual adjustment of the initial structure towards a stable state in solution [16]. From approximately 25 ns onwards, the RMSD reaches a plateau oscillating between approximately 3.0 and 3.5 Å. The protein therefore adopts a globally stable conformation with no significant drift over the remainder of the trajectory.

In this complex, the RMSD of the ligand (LIG26) shows a similar evolution to that of the protein, with generally lower values. For the ligand, the increase in RMSD is linked to a gradual adjustment of its structure within the catalytic pocket. The RMSD of the ligand shows a plateau varying between approximately 2.5 and 3.0 Å. Simultaneous plateau formation for the protein and ligand indicates the establishment of a stable equilibrium [17], in which the ligand remains firmly anchored in the active site while following the overall movements of the receptor. This type of RMSD profile is a strong indicator of conformational stability and simulation convergence [18].

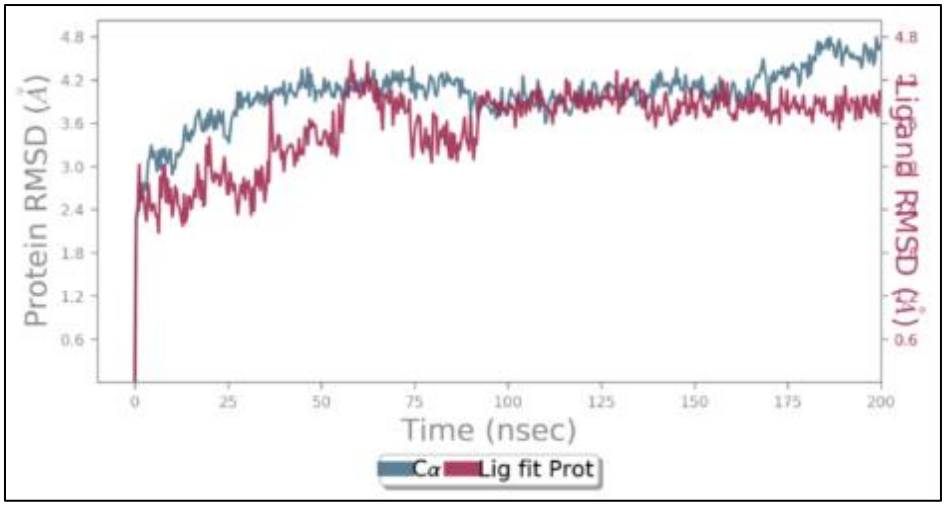


**Figure 3** Evolution of the RMSD of the C-KIT-LIG24 complex

As for the protein–LIG24 complex, its RMSD evolves in a similar way to that of the C-KIT-LIG26 complex. The increase observed at the beginning is followed by a higher plateau. After approximately 10–20 ns, the RMSD of the protein stabilizes between ~3.5 and 4.2 Å. This range of variation is greater than that observed for the protein with the LIG26 ligand. However, their consistency throughout the simulation indicates satisfactory convergence of the system, without major rearrangement of the structure.

The RMSD of the LIG24 ligand docked to the protein shows moderate and regular fluctuations between 3.0 and 3.5 Å. The absence of erratic peaks or upward drift suggests that the ligand remains firmly positioned in the active site throughout the simulation process. The convergence between the RMSD values of the ligand and the protein reflects a concerted dynamic. This can be interpreted as a cohesive interaction in which the ligand follows the overall movements of the receptor **[15]**.

For flexible protein–ligand systems, RMSD values between 3 and 4 Å are considered compatible with dynamic stability when they remain stationary over an extended period **[19]**.

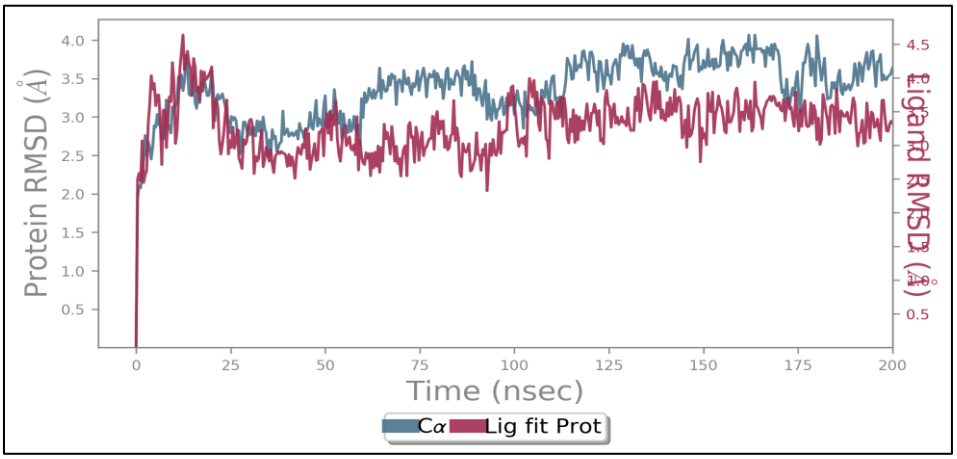


**Figure 4** Evolution of the RMSD of the C-KIT-LIG32 complex

The evolution of the RMSD of the protein–LIG32 complex shows dynamic behavior that is broadly comparable that of the complex with the LIG24 ligand. This evolution manifests itself as a gradual increase over 15 to 20 nanoseconds. After this stage, the RMSD of the protein reaches a plateau with values oscillating between approximately 3.6 and 4.3 Å. A dynamic equilibrium state is rapidly established.

RMSD of the LIG32 ligand stabilizes in the range of approximately 3.1 to 3.6 Å after the initial adjustment phase. These fluctuations remain moderate and regular without abrupt excursions. Occupancy of the active site by this ligand is stable

and long-lasting. The synchronization of the RMSD plateaus reflects a dynamic synergy, frequently associated with good affinity and robust interaction according to the molecular dynamics of protein-ligand complexes **[16]**.

Compared to the two previous complexes, this one has slightly higher RMSD values. However, they remain within an acceptable range for flexible systems, with no significant structural drift.

On the whole, comparing the three complexes shows a consistent overall dynamic. This is marked by an initial relaxation followed by stable RMSD plateaus for the protein and ligands. The protein–LIG26 complex stands out clearly with the lowest RMSD values, reflecting superior dynamic stability. The protein–LIG24 and protein–LIG32 complexes have very similar profiles, with slightly higher but perfectly stationary RMSDs.

It should be noted that the LIG26 ligand with the lowest geometric deviation is also associated with the lowest potential energy (-126,765.893 kcal/mol). This convergence between geometric stability (low and stable RMSD) and energy stability makes the LIG26 ligand the most promising.

Other complementary analyses, such as hydrogen bonds, hydrophobic interactions, and RMSF, were performed. The objective is to identify the fine molecular determinants responsible for the subtle differences in stability observed between the complexes.

### 4.4. Analysis of protein–ligand interactions

Figures 5, 6, and 7 show the contacts established over time between the c-kit protein residues and the ligands LIG26, LIG24, and LIG32, respectively. These contacts are established during a simulation lasting 200 nanoseconds.

Figure 5A shows that the number of contacts between protein residues varies between 3 and 8 during the simulation. The most persistent involve the three residues GLU640, ILE789, and ASP810. ARG791 establishes contacts intermittently. Figures 5B and 5C show the network of molecular interactions involving hydrogen bonds, electrostatic interactions, hydrophobic interactions, and π-cation interactions. Figure 5B shows that the three residues GLU640, ILE789, and ASP810 interact mainly through the formation of hydrogen bonds.

The carboxylate group of the GLU640 residue forms a strong hydrogen bond with the amide group of the ligand with a probability of occurrence of 96%. This bond results from an electrostatic interaction between the carboxylate anion and the hydrogen of the electron-deficient amide function. The ASP810 residue, although negatively charged, forms a hydrogen bond involving a hydrogen atom from its side chain. This bond is formed with the oxygen atom of the amide group of the ligand with a frequency of 68%. It helps to consolidate the ligand's anchorage in the catalytic pocket **[20]**. In addition, the isoleucine residue (ILE789), which is generally hydrophobic, forms a stable hydrogen bond (89%) with the secondary amide group (-NH-) of the ligand via the amide group of its peptide backbone. This backbone-ligand interaction contributes to the stability of the complex within the site. Finally, ARG791, which has a positive charge, participates in a π-cation interaction with the aromatic nucleus of benzothiazole, with a probability of 20%. This interaction is crucial for molecular recognition via the electronic delocalization of the conjugated system **[21]**.

These main interactions are part of a complex structural dynamic, marked by the coexistence of persistent and transient contacts. While GLU640, ASP810, and ILE789 form the interactional core that ensures the complex's long-term stabilization, other residues such as THR670, TYR570, ILE571, ASP572, VAL603, ALA621, LYS623, VAL643, and HIS790 establish only transient contacts, reflecting the dynamic and conformational flexibility of the active site. Specifically, ARG791 only becomes fully involved after 75 ns, indicating a gradual adjustment of the local conformation of the receptor. This alternation between stability and flexibility suggests spatial exploration of the ligand in the binding pocket, allowing fine adaptation to micro variations in the protein environment.

In this way, the cooperation between persistent and transient interactions illustrates the duality of LIG26's behavior : persistent interactions ensure stable affinity of the complex, while modulated interactions reflect its structural adaptability. This coupling of electrostatic (GLU640, ASP810) and hydrophobic (ILE789) interactions, reinforced by π-cation effects (ARG791), gives the whole a multifactorial stability based on the chemical complementarity between the ligand and the receptor.

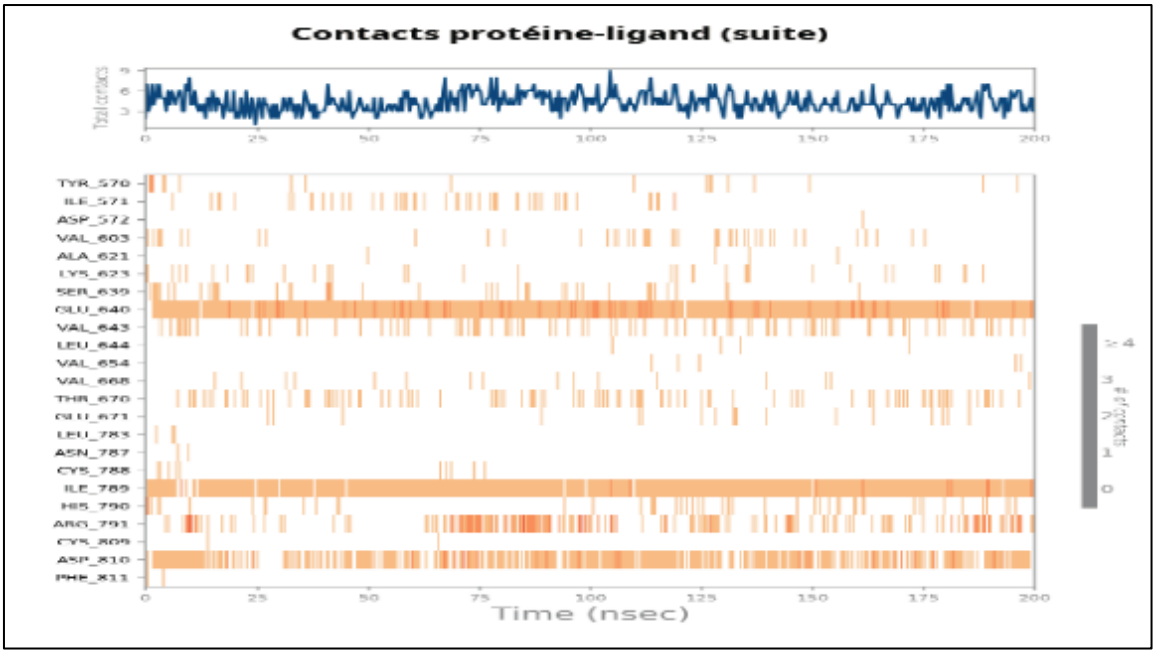


A

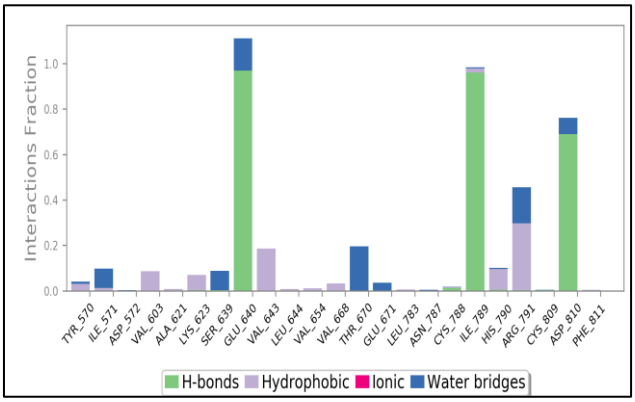


B

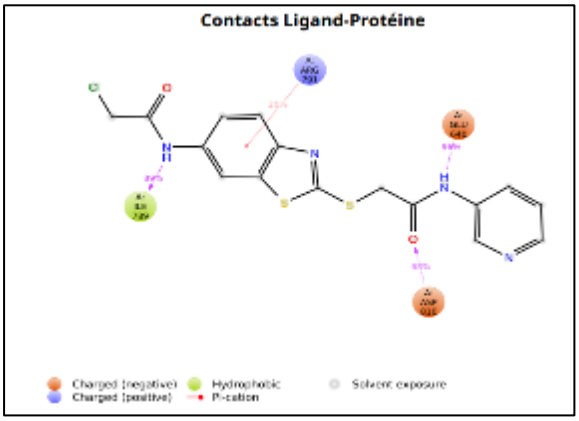


C

**Figure 5** Evolution of the number and persistence of contacts (A) followed by the types of interactions (B) and (C) between LIG26 and the residues of the active site of c-kit during the 200 ns simulation

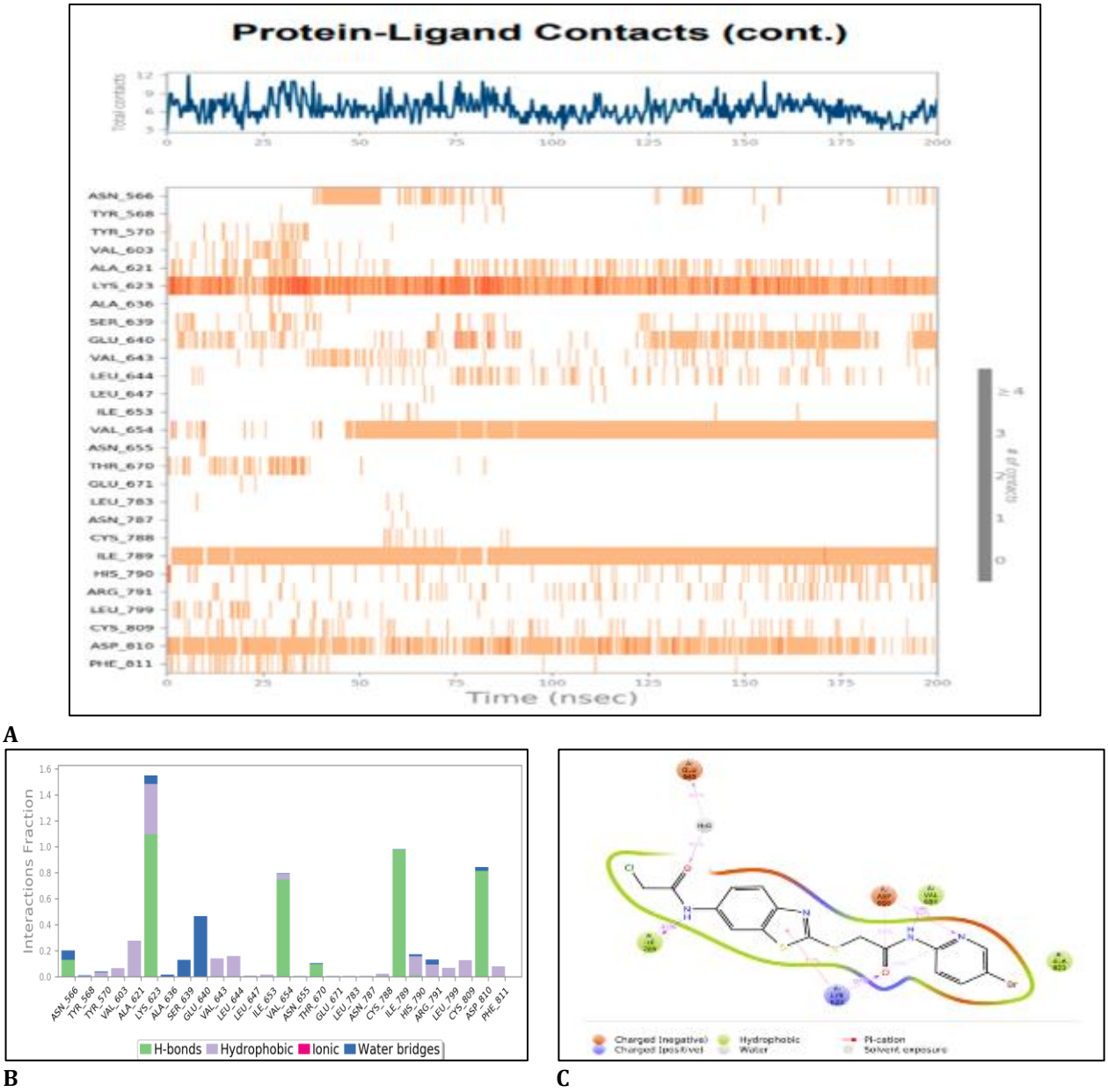


**Figure 6** Evolution of the number and persistence of contacts (A) and then types of interactions (B) and (C) between LIG24 and residues of the active site of c-kit during the 200 ns simulation

Figure 6A indicates that the number of simultaneous residual contacts fluctuates on average between 6 and 7 during the simulation period (200 ns).

The residues LYS623, ILE789, and ASP810 exhibit persistent and intense contacts. They play a central role in stabilizing the complex. Specifically, the LYS623 ligand acts as the main anchor point due to the presence of multiple contacts (electrostatic interactions, cation–π hydrogen bonds). Protein residue ILE789 contributes through hydrogen bonding. This involves the peptide backbone. As for amino acid ASP810, it participates in a stable manner with a slight irregularity at the end of the trajectory.

Residue VAL654 interacts from 45 to 50 ns. This interaction is maintained until the end of the simulation. This behavior reflects a conformational rearrangement by an induced mechanism **[22]**. Residues THR670 and TYR570 are only involved at the beginning of the simulation (0–40 ns). These residues play a role in the initial stabilization of the ligand. Residues such as ASN566 and GLU640 exhibit intermittent contacts, reflecting the local flexibility of the active site. Although less persistent, these transient interactions contribute to the overall stabilization of the complex **[23]**.

In addition, there is a hydrophobic network involving several residues such as LYS623, ALA621, VAL643, LEU644, HIS790, ARG791, CYS809, LEU799, ASP810, PHE811, VAL603, and TYR570. It promotes the partial exclusion of free water from the cavity. This phenomenon contributes to the entropic gain of the complex. The organization of the hydrophobic network consolidates structural cohesion and limits excessive fluctuations of the ligand in the active site **[24]**.

Interactions mediated by water bridges involving residues such as ASN566, ALA636, SER639, GLU640, HIS790, ARG791, and ASP810 are identified. GLU640 makes a notable contribution. These residues play a dynamic adjustment role. Water molecules in the bridges between the ligand and the protein are recognized as key elements of molecular recognition in biological systems **[25]**.

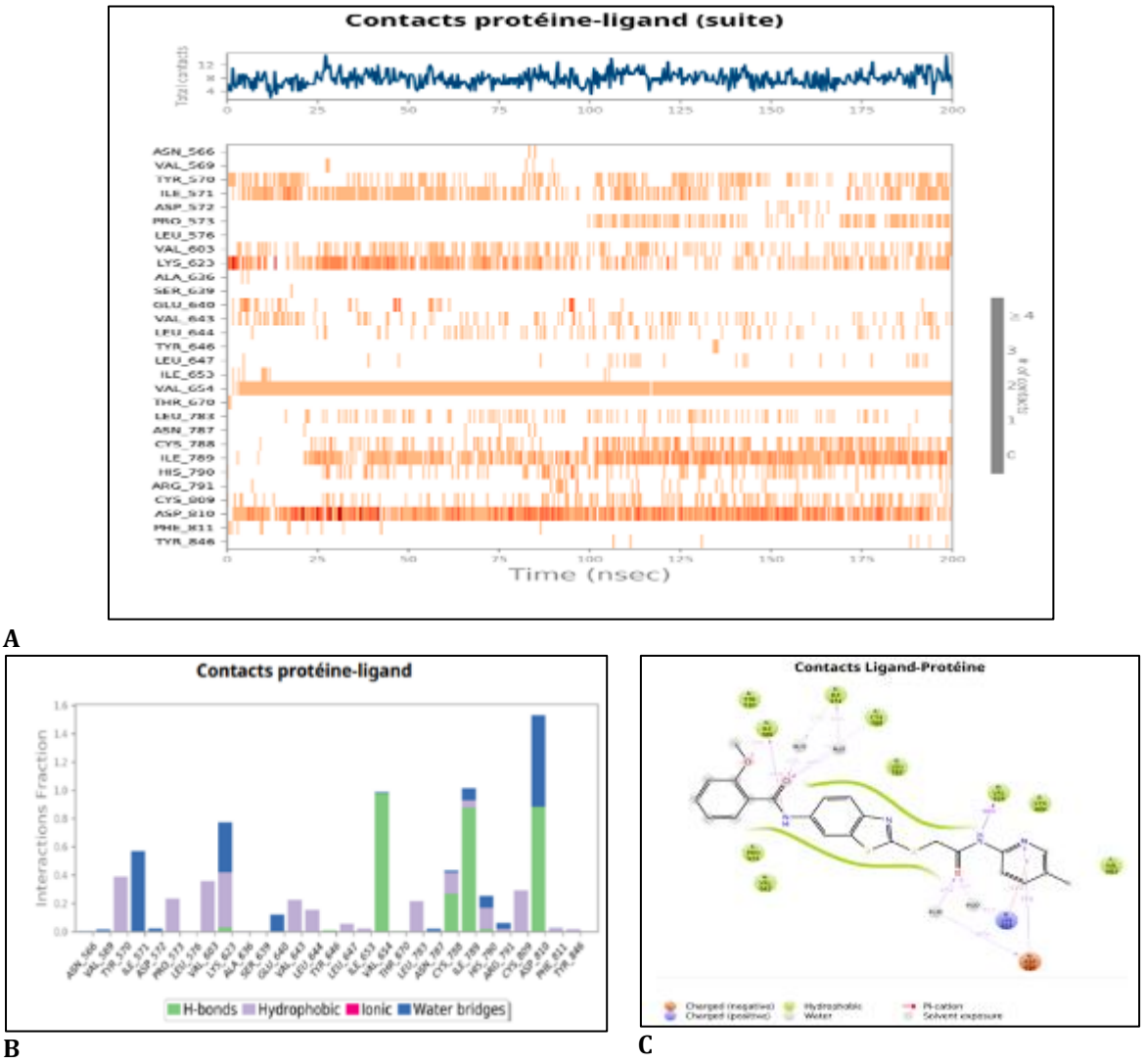


**Figure 7** Evolution of the number and persistence of contacts (A) and then types of interactions (B) and (C) between LIG32 and residues of the active site of c-kit during the 200 ns simulation

The evolution of the total number of contacts during the simulation reveals remarkable stability of the complex [26]. The average number of interaction contacts fluctuates between 8 and 9. These contacts are quasi-permanent during the simulation (200 ns). This persistence of said interactions suggests sustained affinity of the ligand.

Analysis of interaction types shows that hydrogen bonds contribute significantly to the stability of the complex [27]. The residues ASP810, ILE789, VAL654, and LYS623 are repeatedly involved in these interactions. Among these, VAL654 and ASP810 are the basic elements of the complex's stability. The VAL654 residue plays a fundamental role through a persistent hydrogen bond with the amide nitrogen of the ligand for approximately 98% of the simulation time. As for the ASP810 residue, it has an interaction fraction greater than 1 (72% and 47%). It reflects the simultaneous formation

of several contacts, including direct hydrogen bonds and water bridges with the pyridine ring and oxygen of the ligand's amide groups.

Another type of frequent interaction is hydrophobic in nature. These involve the residues TYR570, VAL643, ILE, LEU644, TRP, PRO573, LYS623, VAL654, VAL668, HIS790, and ARG791. These nonpolar interactions contribute to the creation of an environment conducive to ligand insertion into the catalytic pocket. Among these residues, LYS623 stands out for its significant contribution. It establishes a specific π-cation interaction with the pyridine ring of the ligand. This electrostatic interaction, although less frequent, remains significant. It can influence selectivity as well as binding affinity. Thus, LYS623 simultaneously ensures structural stabilization of the complex and plays a decisive role in molecular recognition [28]. All of these hydrophobic interactions reinforce the overall stability of the complex.

Water bridges, although less common, also contribute to the stabilization of the complex. Residues such as VAL643, ILE571, LYS623, ASP810, and GLU640 interact with the ligand via this type of bridge. They optimize polar interactions when direct ligand-residue distances are unfavorable [29].

### 4.5. Analysis of atomic fluctuation of complexed ligands

Root Mean Square Fluctuation (RMSF) profiles were analyzed to evaluate the atomic mobility of the three ligands when complexed to the protein during molecular dynamics simulation. RMSF is a key indicator of local atomic flexibility. It allows regions that are rigidly anchored in the binding pocket to be identified, as opposed to more exposed segments **[16, 19]**. Figures 8, 9, and 10 show the evolution of the RMSF of these ligands.

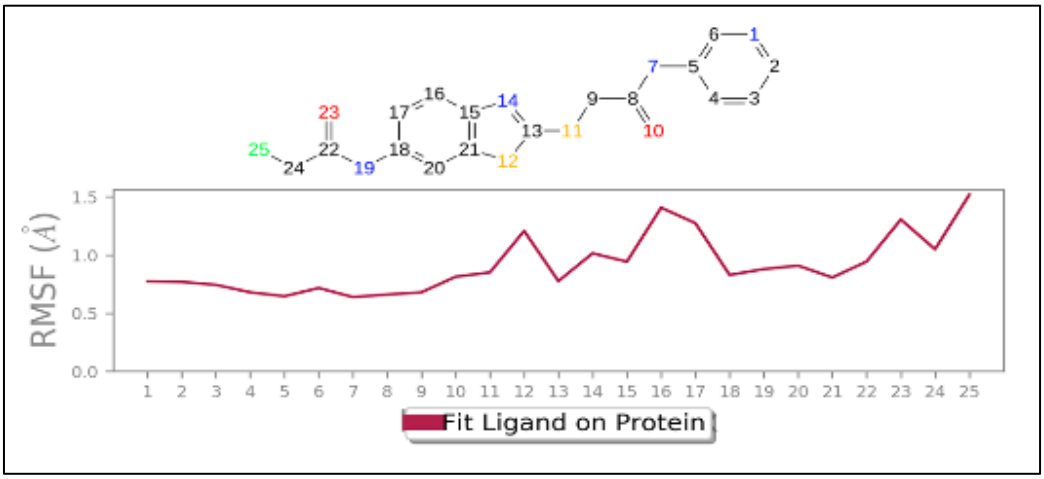


**Figure 8** Variations in the RMSF of ligand 26 during the simulation

Ligand 26 exhibits an overall stable profile during the simulation. A gradual increase in atomic mobility toward the ends is observed. Atoms 1 to 10 show position fluctuations of less than 1.0 Å. This reflects effective anchoring of the benzene ring and adjacent region ((–CONH–) within the active site. This low mobility suggests persistent stabilizing interactions with the surrounding protein residues Glu640 and ASP810.

Meanwhile, a transition zone is seen between atoms 11 and 17, where moderate RMSF peaks appear. These are specifically atoms 12(S) and 16–17 (C16=C17). This increase in flexibility likely reflects intermittent interactions with the protein. Finally, the terminal region (–CONH–Cl) of the ligand exhibits fluctuations reaching approximately 1.5 Å. This observation indicates increased mobility of the terminal chain. This mobility can be explained by less restrictive exposure of the ligand in this region of the binding pocket.

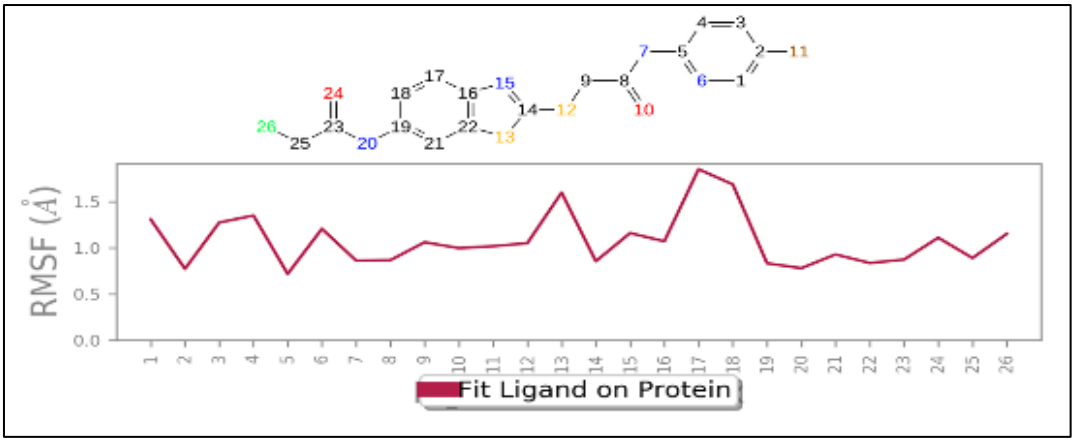


**Figure 9** Variations in the RMSF of ligand 24 during the simulation

Compared to ligand 26, ligand 24 has a much more erratic RMSF profile, suggesting greater structural instability. Atoms numbered 1 to 6 of the ligand (aromatic ring) show high fluctuations of up to 1.4 Å. This shows that this region isn't tightly bound in the protein pocket.

In addition, particularly pronounced mobility peaks are detected around atoms 13 and 17–18, with RMSF values exceeding 1.5 Å. These high fluctuations may be associated with functional groups that are unable to form stable bonds. The other end of the ligand, with atoms 19 to 24, shows relative stability. This area exhibits behavior contrary to that of ligand 26.

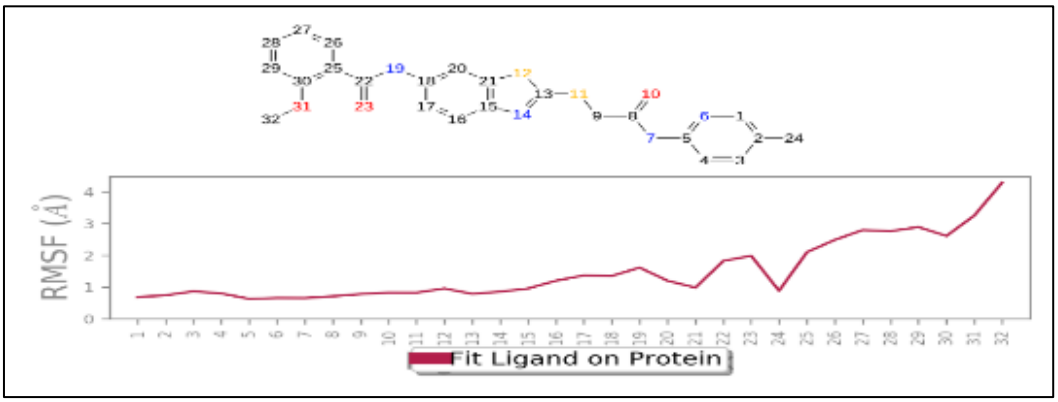


**Figure 10** Variations in the RMSF of ligand 32 during the simulation

Ligand 32 has a very different RMSF profile from the other two. The region comprising atoms 1 to 15 shows remarkable stability with values close to 0.8 Å. This indicates that the aromatic rings are very firmly anchored in the active site.

Starting with atom 25, there is a sharp increase in RMSF fluctuations. Values can reach 4.0 Å. Such an amplitude is typical of a highly flexible region and can be explained by the extension of the terminal chain carrying the methoxy group (–$OCH_3$). This substituent, characterized by a mesomeric donor effect (+M), would modify the local electron distribution. This hydrophilic zone forms hydrogen bonds with water molecules. These weak, short-lived interactions do not immobilize the terminal chain but maintain a rapid association/dissociation dynamic with water, thereby contributing to high conformational flexibility **[30]**. Among the three ligands, LIG26 has the least erratic RMSF profile. It establishes good anchoring of the aromatic nucleus and moderate, progressive flexibility of the terminal chain. Ligand 24, on the other hand, shows instability throughout its structure. Ligand 32 stands out for its excellent anchoring of the proximal region, offset by extreme instability in the distal chain.

## 5. Conclusion

This study used computational strategies to evaluate the potential of three benzothiazole-2-thiol derivatives used as ligands (LIG24, LIG26, and LIG32) for the c-kit tyrosine kinase receptor. The pharmacokinetic profiles and dynamic stability under conditions close to physiological conditions for these derivatives were determined simultaneously.

Initially, ADME analyses and DFT calculations were performed on the three ligands. Combining the results obtained from these two approaches revealed properties that are generally compatible for therapeutic application of these ligands. However, certain limitations were identified. This is the case for the topological polar surface of both LIG26 and LIG32. This surface is likely to influence their membrane permeability.

Secondly, a molecular dynamics simulation of each ligand was performed over a period of 200 ns. These simulations revealed satisfactory structural stability for the three complexes studied. Indeed, the RMSD profiles show plateaus and negative average energy values that are very low. However, a comparative analysis reveals that the C-KIT–LIG26 complex stands out. Indeed, it has the lowest potential energy, lower and more stable RMSD values, and a particularly persistent network of interactions involving key residues of the active site, notably LYS623, ILE789, ASP810, and GLU640. These interactions are based on a synergistic combination of hydrogen bonds, electrostatic interactions, and π-cation contributions, thereby strengthening the cohesion of the complex.

Moreover, RMSF analysis confirms this trend for the LIG26 ligand. It highlights a solid anchoring of the aromatic nucleus of LIG26 within the catalytic pocket, associated with moderate terminal flexibility. This behavior reflects an optimal balance between structural rigidity and conformational adaptability. This balance is essential for dynamic adjustment in the protein environment.

In summary, all these results indicate that the LIG26 ligand is the best candidate for developing a c-kit-targeting inhibitor for the treatment of hepatocellular carcinoma.

## Compliance with ethical standards

*Disclosure of conflict of interest*

No conflict of interest to be disclosed.

## References

[1] Lennartsson, J., & Rönnstrand, L. Stem Cell Factor Receptor/c-kit : From Basic Science to Clinical Implications. Physiological Reviews. 2012a; 92(4): 1619-1649. https://doi.org/10.1152/physrev.00046.2011

[2] Demetri, G. D., Von Mehren, M., Blanke, C. D., Van Den Abbeele, A. D., Eisenberg, B., Roberts, P. J., and al. Efficacy and Safety of Imatinib Mesylate in Advanced Gastrointestinal Stromal Tumors. New England Journal of Medicine. 2002; 347(7): 472-480. https://doi.org/10.1056/NEJMoa020461

[3] Wang, Z., Shi, X.-H., Wang, J., Zhou, T., Xu, Y.-Z., Huang, T.-T., and al. Synthesis, structure–activity relationships and preliminary antitumor evaluation of benzothiazole-2-thiol derivatives as novel apoptosis inducers. Bioorganic & Medicinal Chemistry Letters .2011; 21(4) : 1097-1101. https://doi.org/10.1016/j.bmcl.2010.12.124

[4] Heinrich, M. C., Corless, C. L., Duensing, A., McGreevey, L., Chen, C.-J., Joseph, N., and al. PDGFRA Activating Mutations in Gastrointestinal Stromal Tumors. Science. 2003; 299(5607): 708-710. https://doi.org/10.1126/science.1079666

[5] Lennartsson, J., & Rönnstrand, L. Stem Cell Factor Receptor/c-kit : From Basic Science to Clinical Implications. Physiological Reviews.2012b;92(4): 1619-1649. https://doi.org/10.1152/physrev.00046.2011

[6] Demetri, G. D., von Mehren, M., Blanke, C. D., Van den Abbeele, A. D., Eisenberg, B., Roberts, P. J., Heinrich, M. C., and al. Efficacy and safety of imatinib mesylate in advanced gastrointestinal stromal tumors. The New England Journal of Medicine. 2002; 347(7): 472-480. https://doi.org/10.1056/NEJMoa020461

[7] Daina, A., Michielin, O., & Zoete, V. SwissADME : A free web tool to evaluate pharmacokinetics, drug-likeness and medicinal chemistry friendliness of small molecules. Scientific Reports. 2017; 7(1), 42717. https://doi.org/10.1038/srep42717

[8] Becke, A. D. Density-functional thermochemistry. III. The role of exact exchange. The Journal of Chemical Physics. 1993; 98(7): 5648-5652. https://doi.org/10.1063/1.464913

[9] Jorgensen, W. L., Chandrasekhar, J., Madura, J. D., Impey, R. W., & Klein, M. L. Comparison of simple potential functions for simulating liquid water. The Journal of Chemical Physics.1983;79(2): 926-935. https://doi.org/10.1063/1.445869

[10] Arnott, J. A., & Planey, S. L. The influence of lipophilicity in drug discovery and design. Expert Opinion on Drug Discovery. 2012; 7(10): 863-875. https://doi.org/10.1517/17460441.2012.714363

[11] Veber, D. F., Johnson, S. R., Cheng, H.-Y., Smith, B. R., Ward, K. W., & Kopple, K. D. Molecular Properties That Influence the Oral Bioavailability of Drug Candidates. Journal of Medicinal Chemistry.2002;45(12):2615-2623. https://doi.org/10.1021/jm020017n

[12] Ertl, P., Rohde, B., & Selzer, P. Fast Calculation of Molecular Polar Surface Area as a Sum of Fragment-Based Contributions and Its Application to the Prediction of Drug TransportProperties. Journal of Medicinal Chemistry. 2000; 43(20): 3714-3717. https://doi.org/10.1021/jm000942e

[13] Levitt, M., & Warshel, A. Computer simulation of protein folding. Nature. 1975; 253(5494): 694-698. https://doi.org/10.1038/253694a0

[14] Berendsen, H. J. C., Postma, J. P. M., Van Gunsteren, W. F., DiNola, A., & Haak, J. R. Molecular dynamics with coupling to an external bath. The Journal of Chemical Physics. 1984; 81(8): 3684-3690. https://doi.org/10.1063/1.448118

[15] De Vivo, M., Masetti, M., Bottegoni, G., & Cavalli, A. Role of Molecular Dynamics and Related Methods in Drug Discovery. Journal of Medicinal Chemistry. 2016; 59(9): 4035-4061. https://doi.org/10.1021/acs.jmedchem.5b01684

[16] Karplus, M., & McCammon, J. A. Molecular dynamics simulations of biomolecules. Nature Structural Biology.2002a; 9(9): 646-652. https://doi.org/10.1038/nsb0902-646

[17] Walton, E. B. Équilibrage de structures protéiques déterminées expérimentalement pour la simulation de dynamique moléculaire. Physical Review E.2006; 74(6). https://doi.org/10.1103/PhysRevE.74.061901

[18] Schreiner, W., Karch, R., Knapp, B., & Ilieva, N. Relaxation estimation of RMSD in molecular dynamics immunosimulations. Computational and Mathematical Methods in Medicine.2012; 2012: 173521. https://doi.org/10.1155/2012/173521

[19] Hollingsworth, S. A., & Dror, R. O. Molecular Dynamics Simulation for All. Neuron. 2018; 99(6), 1129-1143. https://doi.org/10.1016/j.neuron.2018.08.011

[20] Salentin, S., Schreiber, S., Haupt, V. J., Adasme, M. F., & Schroeder, M. PLIP : Fully automated protein–ligand interaction profiler. Nucleic Acids Research. 2015; 43(W1): W443-W447. https://doi.org/10.1093/nar/gkv315

[21] Kitchen, D. B., Decornez, H., Furr, J. R., & Bajorath, J. Docking and scoring in virtual screening for drug discovery : Methods and applications. Nature Reviews Drug Discovery.2004; 3(11): 935-949. https://doi.org/10.1038/nrd1549

[22] Gallivan, J. P., & Dougherty, D. A. Cation-π interactions in structural biology. Proceedings of the National Academy of Sciences.1999; 96(17):9459-9464. https://doi.org/10.1073/pnas.96.17.9459

[23] Henzler-Wildman, K., & Kern, D. Dynamic personalities of proteins. Nature. 2007; 450(7172): 964-972. https://doi.org/10.1038/nature06522

[24] Manukhin, B. N. Analysis of Ligand-Receptor Interactions from the Molecular Level to the Whole-Body Level. Neuroscience and Behavioral Physiology.2002; 32(3): 283-291. https://doi.org/10.1023/A:1015014408089

[25] Ladbury, J. E. Just add water ! The effect of water on the specificity of protein-ligand binding sites and its potential application to drug design. Chemistry & Biology.1996; 3(12): 973-980. https://doi.org/10.1016/S1074-5521(96)90164-7

[26] Gelpi, J., Hospital, A., Goñi, R., & Orozco, M. Molecular dynamics simulations : Advances and applications. Advances and Applications in Bioinformatics and Chemistry. 2015; 37. https://doi.org/10.2147/AABC.S70333

[27] Hubbard, R. E. Hydrogen Bonds in Proteins : Role and Strength. In Wiley, Encyclopedia of Life Sciences. 2001; (1re éd.). Wiley. https://doi.org/10.1038/npg.els.0003011

[28] Meyer, E. A., Castellano, R. K., & Diederich, F. Interactions with Aromatic Rings in Chemical and Biological Recognition. Angewandte Chemie International Edition. 2003; 42(11): 1210-1250. https://doi.org/10.1002/anie.200390319

[29] Hüfner-Wulsdorf, T., & Klebe, G. Role of Water Molecules in Protein-Ligand Dissociation and Selectivity Discrimination : Analysis of the Mechanisms and Kinetics of Biomolecular Solvation Using Molecular Dynamics. Journal of Chemical Information and Modeling. 2020; 60(3):1818-1832. https://doi.org/10.1021/acs.jcim.0c00156

[30] Karplus, M., & McCammon, J. A. Molecular dynamics simulations of biomolecules. Nature Structural Biology.2002b; 9(9): 646-652. https://doi.org/10.1038/nsb0902-646